Recent developments on adaptive fast Boundary Element Methods to model elastic wave propagation in sedimentary basins

Faisal Amlani, Stéphanie Chaillat, Adrien Loseille

CSMA 2019
14ème Colloque National en Calcul des Structures
13-17 Mai 2019, Presqu'île de Giens (Var)

Recent developments on adaptive fast Boundary Element Methods to model elastic wave propagation in sedimentary basins

F. Amlani[1], S. Chaillat[1], A. Loseille[2]

[1] *POEMS, ENSTA-UMA, {amlani,chaillat}@ensta.fr*
[2] *INRIA Saclay Ile-de-France, adrien.loseille@inria.fr*

Résumé — The main advantage of the Boundary Element Method (BEM) is that only the domain boundaries are discretized. It is thus well-suited to study site effects. This advantage is offset by the full BEM matrix. In the last couple of years, fast BEMs have been proposed to overcome this drawback. If the efficiency of fast BEMs has been demonstrated, the iteration count becomes now the main limitation to consider realistic problems. Mesh adaptation is an additional technique to reduce the computational cost and number of iterations of the BEM. In this contribution, we give an overview of recent works to speed-up fast BEMs, i.e. an anisotropic metric-based mesh adaptation technic.
Mots clés — Boundary Element Method, Wave propagation, Mesh adaptation.

1 Modelling elastic wave propagation in sedimentary basins

The motivation of this work is the modelling of the amplification of the seismic motion while traveling the different layers of the soil to understand *site effects* and *soil-structure interactions* (see Figure 1).

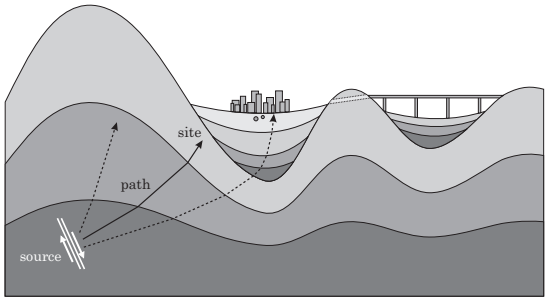

FIGURE 1 – The seismic waves can be amplified by the geological and topographical structure of the soil (site effects) and this amplified motion interacts with the structures in the city (soil-structure interactions) (figure from [9]).

The propagation of elastic waves can be simulated by means of various numerical methods : finite element method (FEM), finite difference method, spectral element method, Discontinuous Galerkin method, Boundary Element Method (BEM) [4], ... The latter, which corresponds to the numerical solution of boundary integral equations, has the advantages of necessitating only the discretization of the boundary of the computational domain and intrinsically taking into account radiation conditions in the formulation. The main drawbacks of the BEM are : (i) that it requires the knowledge or numerical evaluation of the fundamental solution and (ii) that it leads to a smaller size problem (compared to volume methods) but with a fully-populated linear system. This system can be solved with either direct or iterative solvers but the $O(N^2)$ complexity in terms of memory requirements is always prohibitive to apply BEMs to very large-scale problems. The solution of realistic configurations in terms of geometry, heterogeneity, frequency range, ... is therefore limited by the number of degrees of freedom that the solver can handle on a given computer.

For all these reasons, fast BEMs have undergone intense development in the last 30 years. The principle of fast BEMs such as the fast multipole accelerated BEM (FM-BEM) or the $\mathcal{H}$-matrix based BEM ($\mathcal{H}$-BEM) is to speed up the integral operator evaluations entailed by matrix-vector products. These

methods are thus intrinsically based on the use of an iterative solver. The efficiency of fast BEMs has been demonstrated for elastic wave propagation including in sedimentary basins [6, 5]. However, the iteration count of the iterative solver becomes now the main limitation to consider realistic problems. This number of iterations has been shown to increase with the problem size, frequency and number of layers in the case of sedimentary basins. The definition of efficient preconditioners for fast BEMs is a timely and difficult subject. Thus, to reduce computational times, the system matrix is never explicitly assembled. Standard preconditioning strategies proposed in the context of FEM cannot be directly applied.

Mesh adaptation is an additional (complementary) technique to reduce the computational cost of fast BEMs. The principle is to optimize (or at least improve) the positioning of a given number of degrees of freedom on the geometry, in order to yield simulations with superior accuracy compared to those obtained via the use of uniform meshes. If an extensive literature is available for volume methods, much less attention has been devoted to BEMs. In this contribution, we give an overview of recent works to speed-up the solution of 3D acoustic and elastodynamic BEMs. More precisely, we will present an anisotropic metric-based mesh adaptation technic.

2 The Boundary Element Method and its acceleration with Fast Boundary Element Methods

Boundary integral representation and boundary integral equation (BIE). The BIE formulation for frequency-domain elastodynamics is summarized in its basic form. Assume for definiteness that time-harmonic motions, with circular frequency ω, are induced by a prescribed traction distribution $\boldsymbol{t}^{\mathrm{D}}$ on the boundary $\partial\Omega$ and in the absence of body forces (with straightforward modifications allowing the discussion of other boundary conditions or other integral formulations). The displacement $\boldsymbol{u}$ is given at an interior point $\boldsymbol{x} \in \Omega$ by the following representation formula :

$$\boldsymbol{u}(\boldsymbol{x}) = -\int_{\partial\Omega} \boldsymbol{u}(\boldsymbol{y})\cdot\boldsymbol{T}(\boldsymbol{x},\boldsymbol{y})\,\mathrm{d}S_y + \int_{\partial\Omega} \boldsymbol{t}^{\mathrm{D}}(\boldsymbol{y})\cdot\boldsymbol{U}(\boldsymbol{x},\boldsymbol{y})\,\mathrm{d}S_y \qquad (\boldsymbol{x}\in\Omega), \tag{1}$$

where $\boldsymbol{U}(\boldsymbol{x},\boldsymbol{y})$ and $\boldsymbol{T}(\boldsymbol{x},\boldsymbol{y})$ denote an elastodynamic Green's tensor. The simplest, and most commonly used, Green's tensor corresponds to the isotropic full-space :

$$\begin{aligned} \boldsymbol{U}(\boldsymbol{x},\boldsymbol{y}) &= \frac{1}{\kappa_{\mathrm{S}}^2\mu}\Big[\big(\boldsymbol{I}\Delta - \boldsymbol{\nabla}_y\boldsymbol{\nabla}_x\big)G(|\boldsymbol{y}-\boldsymbol{x}|;\kappa_{\mathrm{S}}) + \boldsymbol{\nabla}_x\boldsymbol{\nabla}_y G(|\boldsymbol{y}-\boldsymbol{x}|;\kappa_{\mathrm{P}})\Big], \\ \boldsymbol{T}(\boldsymbol{x},\boldsymbol{y}) &= \boldsymbol{n}(\boldsymbol{y})\cdot\mathcal{C}:\boldsymbol{\nabla}_y\boldsymbol{U}(\boldsymbol{x},\boldsymbol{y}), \end{aligned} \tag{2}$$

where $\boldsymbol{n}(\boldsymbol{y})$ is the unit normal to $\partial\Omega$ directed outwards of Ω and $G(\cdot;\kappa)$ is the free-space fundamental solution for the Helmholtz equation with wavenumber κ, given by

$$G(r;\kappa) = \frac{\exp(\mathrm{i}\kappa r)}{4\pi r}, \quad \text{with } r = ||\boldsymbol{x}-\boldsymbol{y}||. \tag{3}$$

Well-known results on the limiting values of elastic potentials as the point $\boldsymbol{x}$ reaches the boundary allow to deduce from (1) the boundary integral equation

$$\mathcal{K}[\boldsymbol{u}](\boldsymbol{x}) = \mathcal{S}[\boldsymbol{t}^{\mathrm{D}}](\boldsymbol{x}) \quad (\boldsymbol{x}\in\partial\Omega) \qquad \text{with } \mathcal{K}[\boldsymbol{u}](\boldsymbol{x}) := \mathcal{D}[\boldsymbol{u}](\boldsymbol{x}) + \boldsymbol{c}(\boldsymbol{x})\cdot\boldsymbol{u}(\boldsymbol{x}), \tag{4}$$

where the right-hand side and the linear operator $\mathcal{K}$ respectively involve the single-layer integral operator $\mathcal{S}$ and the double-layer integral operator $\mathcal{D}$, defined by

$$\mathcal{S}[\boldsymbol{t}](\boldsymbol{x}) := \int_{\partial\Omega} \boldsymbol{t}(\boldsymbol{y})\cdot\boldsymbol{U}(\boldsymbol{x},\boldsymbol{y})\,\mathrm{d}S_y, \quad \mathcal{D}[\boldsymbol{u}](\boldsymbol{x}) := (\mathrm{P.V.})\int_{\partial\Omega} \boldsymbol{u}(\boldsymbol{y})\cdot\boldsymbol{T}(\boldsymbol{x},\boldsymbol{y})\,\mathrm{d}S_y, \quad \boldsymbol{x}\in\partial\Omega. \tag{5}$$

Due to the strong singularity of $\boldsymbol{T}$ for $\boldsymbol{y}=\boldsymbol{x}$, the integral defining $\mathcal{D}$ is understood in the Cauchy principal value (CPV) sense (as indicated by the notation P.V.) while a *free-term* $\boldsymbol{c}(\boldsymbol{x})$ arose from the limit-to-the-boundary process. The latter is equal to $0.5\boldsymbol{I}$ in the usual case where $\partial\Omega$ is smooth at $\boldsymbol{x}$, and is otherwise a known (second-order tensor-valued) function of the local geometry of $\partial\Omega$ at $\boldsymbol{x}$.

Boundary Element Method. The main ingredients of the numerical solution of boundary integral equation (4) are a transposition of the concepts developed for the Finite Element Method. It is based on a discretization of the surface $\partial\Omega$ into N_E isoparametric boundary elements of order one, i.e. three-node triangular elements. Higher order discretizations are also possible. The N interpolation points $\boldsymbol{y}_1, \ldots, \boldsymbol{y}_N$ are chosen as the vertices of the mesh. Each component of the displacement field is approximated with globally continuous, piecewise-linear shape functions. The discretization process of the boundary integral equation (4) is either based on a nodal collocation or on a Galerkin approach. In this work, we consider only the collocation approach but most of the algorithms presented can be extended straightforwardly to the Galerkin approach. The collocation consists in enforcing the equation at a finite number of collocation points $\boldsymbol{x}$. To have a solvable discrete problem, one has to choose N collocation points. The N displacement approximation nodes thus defined also serve as collocation points, i.e. $(\boldsymbol{x}_i)_i = (\boldsymbol{y}_j)_j$. This discretization process transforms (4) into a square complex-valued linear system of size $3N$ of the form

$$\mathbb{K}\mathbf{u} = \mathbf{f}, \tag{6}$$

where the $3N$-vector $\mathbf{u}$ collects the sought degrees of freedom (DOFs), namely the nodal displacement components, $\mathbb{K}$ is the $3N \times 3N$ influence matrix and the $3N$-vector $\mathbf{f}$ arises from the discretization of $\mathcal{S}[\boldsymbol{t}^{\mathrm{D}}]$. Setting up the matrix $\mathbb{K}$ classically has a $O(N^2)$ complexity.

The important and limiting aspect in the BEM is that the influence matrix $\mathbb{K}$ is fully-populated. Usual direct solvers, such as the LU factorization, then have a complexity of $O(N^3)$ in terms of computational times and of $O(N^2)$ in terms of memory requirements, limiting the applicability of the traditional BEM to moderately-sized models. BEM problems of larger size are preferably solved by means of iterative algorithms (GMRES for example). Each GMRES iteration requires one evaluation of $\mathbb{K}\mathbf{w}$ for given $\mathbf{w}$, a task of computational complexity $O(N^2)$ whether $\mathbb{K}$.

Fast Multipole accelerated BEM for 3D elastodynamics. The Fast Multipole accelerated BEM consists in formulating sparse approximations of $\mathcal{K}$ by recasting the fundamental solutions, e.g. $\boldsymbol{U}(\boldsymbol{x},\boldsymbol{y})$, $\boldsymbol{T}(\boldsymbol{x},\boldsymbol{y})$ in (1), in terms of products of functions of $\boldsymbol{x}$ and of $\boldsymbol{y}$. On recasting the position vector $\boldsymbol{r} = \boldsymbol{y} - \boldsymbol{x}$ in the form $\boldsymbol{r} = \tilde{\boldsymbol{y}} - \tilde{\boldsymbol{x}} + \boldsymbol{r}_0$, having set $\tilde{\boldsymbol{y}} := \boldsymbol{y} - \boldsymbol{y}_0$, $\tilde{\boldsymbol{x}} := \boldsymbol{x} - \boldsymbol{x}_0$ and $\boldsymbol{r}_0 := \boldsymbol{y}_0 - \boldsymbol{x}_0$ in terms of two chosen poles $\boldsymbol{x}_0$, $\boldsymbol{y}_0$, decompositions of the form FMMs for waves [5] are often based on the fact that the Helmholtz Green's function (3) is known to admit the following plane wave expansion

$$G(|\boldsymbol{r}|;\kappa) = \lim_{L\to+\infty} G_L(|\boldsymbol{r}|;\kappa), \quad \text{with } G_L(|\boldsymbol{r}|;\kappa) := \int_{\hat{S}} e^{\mathrm{i}\kappa\hat{\boldsymbol{s}}\cdot\tilde{\boldsymbol{y}}}\, \mathcal{G}_L(\hat{\boldsymbol{s}};\boldsymbol{r}_0;\kappa) e^{-\mathrm{i}\kappa\hat{\boldsymbol{s}}\cdot\tilde{\boldsymbol{x}}}\, \mathrm{d}\hat{\boldsymbol{s}}, \tag{7}$$

where $\hat{S} \subset \mathbb{R}^3$ is the unit sphere and the *transfer function* $\mathcal{G}_L(\hat{\boldsymbol{s}};\boldsymbol{r}_0;\kappa)$ is defined in terms of the Legendre polynomials P_n and the spherical Hankel functions of the first kind $h_n^{(1)}$ by :

$$\mathcal{G}_L(\hat{\boldsymbol{s}};\boldsymbol{r}_0;\kappa) = \frac{\mathrm{i}\kappa}{16\pi^2} \sum_{0\le n\le L} (2p+1)\mathrm{i}^n h_n^{(1)}(\kappa|\boldsymbol{r}_0|) P_n\big(\cos(\hat{\boldsymbol{s}},\boldsymbol{r}_0)\big). \tag{8}$$

The separated character of expansion (8) allows to re-use integrations with respect to $\boldsymbol{y}$ when the collocation point $\boldsymbol{x}$ is changed. This is one of the main mechanisms for lowering the $O(N^2)$ complexity per iteration entailed by standard BEMs (see Fig. 2).

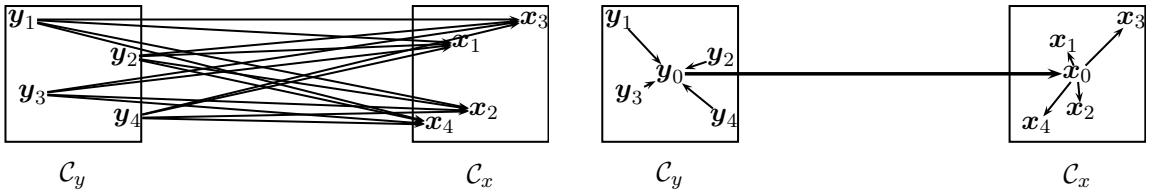

FIGURE 2 – Matrix-vector product with Standard BEM and FM-BEM. The use of the FMM drastically reduces the number of operations necessary to calculate the influence of the source points y_i located in the cell $\mathcal{C}_y$ on the observation points x_i in the cell $\mathcal{C}_x$.

The error introduced by the plane wave expansion is controllable when $\|\tilde{\boldsymbol{x}}\|$, $\|\tilde{\boldsymbol{y}}\|$ are sufficiently small compared to $\|\boldsymbol{r}_0\|$. This naturally leads to subdividing the (collocation, integration) points involved

in the BE-discretized integral equation into clusters and applying decompositions of type (7) to well-separated clusters. This subdivision is usually performed by means of a 3D cubic grid of linear spacing d embedding the geometrical support $\partial\Omega$ of (1), so that $\partial\Omega$ is enclosed in a set of cubic cells. The FMM basically consists in using (7), with the poles $\boldsymbol{x}_0$ and $\boldsymbol{y}_0$ chosen as the cell centers, whenever $\boldsymbol{x}$ and $\boldsymbol{y}$ belong to *non-adjacent* cubic cells. When $\boldsymbol{x}$ and $\boldsymbol{y}$ belong to adjacent cells, the original definitions of the kernels are used. To further improve the computational efficiency of the FM-BEM, standard (i.e. non-FMM) calculations must be confined to the smallest possible spatial regions while retaining the advantage of clustering the computation of influence terms into non-adjacent large groups whenever possible. This is achieved by recursively subdividing cubic cells into eight smaller cubic cells. New pairs of non-adjacent smaller cells, to which the plane expansion is applicable, are thus obtained from the subdivision of pairs of adjacent cells. The cell-subdivision approach is systematized by means of an octree structure of cells. This octree-based recursive clustering, which defines the so-called multi-level FMM, is the other main mechanism for lowering the complexity of BEMs. The theoretical complexity of the multi-level FMM for Helmholtz-type kernels is in fact known to be $O(N\log_2 N)$ per GMRES iteration both for CPU time and memory [5].

3 Anisotropic mesh adaptation for Boundary Element Methods

The principle of mesh adaptation is to optimize the positioning of a given number of degrees of freedom on the geometry of the obstacle, in order to yield simulations with superior accuracy compared to those obtained via the use of uniform meshes. For wave scattering problems, adaptation is particularly important for obstacles that contain geometric singularities, i.e., edges and vertices, which lead to a rapid variation of the surface solution near these singularities. In addition, we may exploit the directionality of the waves in order to further reduce the number of degrees of freedom. The best strategy to achieve these goals is via so-called "anisotropic" mesh adaptation for which an extensive literature exists for volume-based methods [1]. However, there is relatively little research attention being paid to mesh adaptation in a boundary element context. One possible explanation is the large computational cost of standard BEMs. With the development of fast BEMs, the capabilities of the BEMs are greatly improved such that efficient adaptive mesh strategies are needed not only to optimize further the computational cost, but also to certify the numerical results by assessing that the theoretical convergence order is observed during the computations. Most current BEM adaptivity methods, like those relying on Dörfler marking, have been confined to isotropic techniques. In addition, most works are restricted to Galerkin discretizations and are formulated specifically for a system of equations [2, 3].

The first originality of our work is the extension of metric-based anisotropic mesh adaptation (AMA) to the collocation BEM where it has never been used. The metric-based AMA does not employ a Dörfler marking strategy but rather generates a sequence of non-nested meshes with a specified complexity (similar to the prescription of a number of DOFs) [8]. We find the optimal mesh that permits the minimization of the approximation error due to the discretization scheme. More precisely, we try to reduce the linear interpolation error of the (unknown) exact solution on the current mesh. A convenient framework to generate anisotropic meshes is that of Riemannian metric spaces. A Riemannian metric space is defined by a metric tensor $\mathcal{M}(\boldsymbol{x})$. By generating a unit mesh in the corresponding Riemannian metric space, we obtain an anisotropic mesh refined in Euclidean space according to the metric $\mathcal{M}$. This is the fundamental idea of metric-based mesh adaptation. We have shown that the optimal metric $\mathcal{M}^*$ to reduce the interpolate error in L^p-norm in a BEM context is given by [7] :

$$R_s(\mathcal{M}^*) = D^* \ \det(|R_s(H)|)^{\frac{-1}{2(p+1)}} \ |R_s(H)|, \text{ with } D^* = \mathcal{N}\left(\int_\Gamma \det(|R_s(H)|)^{\frac{p}{2(p+1)}}\right)^{-1}$$

where H is the Hessian of the solution, $\mathcal{N}$ is the complexity of a mesh and R_s is a restriction operator (3D$\rightarrow$2D). As a result, in AMA the size, shape, and orientation of elements are adjusted simultaneously. With the minimizing mesh in hand, one repeats the process for larger $\mathcal{N}$ until some ad-hoc stopping criterion is achieved. More precisely, given a user-prescribed sequence of complexity $\boldsymbol{N} = [\mathcal{N}_1, ..., \mathcal{N}_k]$, we seek the sequence of corresponding optimal meshes $\mathcal{T} = [\mathcal{T}_1, ..., \mathcal{T}_k]$. This process is non-linear, i.e., both the mesh and the solution have to be converged. The advantages of this approach are that it is ideally

suited to solutions with anisotropic features, it is independent of the underlying PDE (e.g. acoustics or elastodynamics) and discretization technique (collocation, Galerkin, etc.).

The second originality of our work is the combination of two acceleration techniques, namely metric-based anisotropic mesh adaptivity and Fast Multipole acceleration. If no fast BEM is used, the capabilities of anisotropic mesh techniques cannot be fully demonstrated for realistic large scale scattering scenarios. This original combination permits us to show the performance of AMA strategy for complex real-world problems since it is providing manageable system sizes for a desired accuracy (to achieve the same with a uniform mesh, one may require a discretization exceeding memory capabilities) to the FM-BEM solver.

4 Illustration of the capabilities of the adapted FM-BEM solver for wave propagation problems

The proposed strategy constructs adapted meshes that can be shown to recover optimal convergence rates for domains with corners and edges. As this strategy is new, we consider first simple homogeneous configurations for the Helmholtz equation before to consider the piecewise homogeneous elastic configuration motivating this work (Figure 1). Figure 3 illustrates a corner portion of meshes generated for a planar screen geometry at three iterations of the AMA process. One can observe clear refinement at the edges to handle the geometric and solution singularities. Importantly, the computation of the metric and subsequent generation of the mesh itself is a rather inexpensive calculation, negligible relative to the corresponding FM-BEM solution time (usually less than 5% of the overall computational cost).

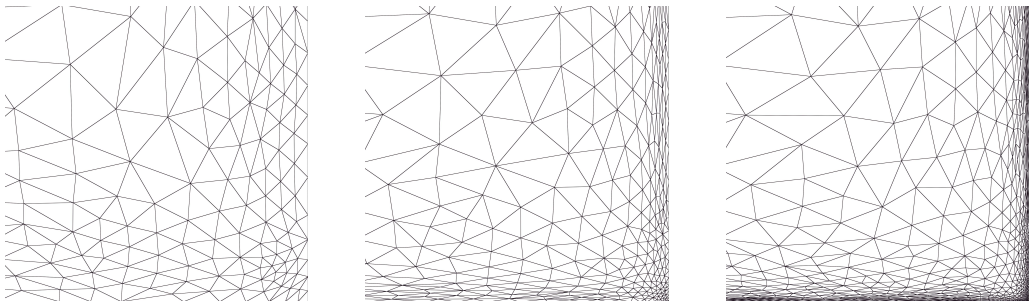

FIGURE 3 – An example of the first, third and fifth iterations (in the mesh adaptation process) employed in the anisotropic screen meshes. The complexities input for each case are $\mathcal{N} = 350, 1400$ and 5600.

To check that the AMA process allows to recover optimal convergence rates, we consider the sound-soft problem of a cube with cavity (Figure 4**a**). The incident direction is $\mathbf{d}^i = (-2,-1,-1)$. The errors for the adapted and uniform meshes are computed on a circle of radius 2 and are shown in Figure 4**b** for the wavenumber $k = 10$. As expected, the uniform refinement yields a suboptimal convergence rate.

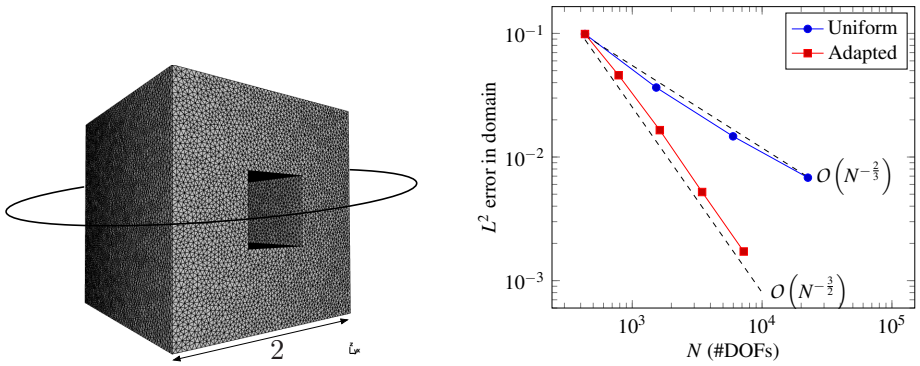

(**a**) (**b**)

FIGURE 4 – *Sound-soft cube with cavity : L^2 errors for uniform and adapted meshes for $k = 10$.*

We then illustrate the robustness of the technique with respect to the complexity of an input geometry. We consider the geometry of the unarmed F-15 aircraft for an incident plane wave with direction $\mathbf{d} = (1/2, 1, 0)^T$ and wavenumber $k = 6$. Figure 5 presents an illustrative discretization of the anisotropic

adaptation on a portion of the wing as well as the boundary solution (real part and complex amplitude). We see the high directionality of the diffracted waves with different patterns for the front and back of the aircraft, and most of the resulting anisotropy in the meshes are reached in areas where the diffracted waves have low regularity.

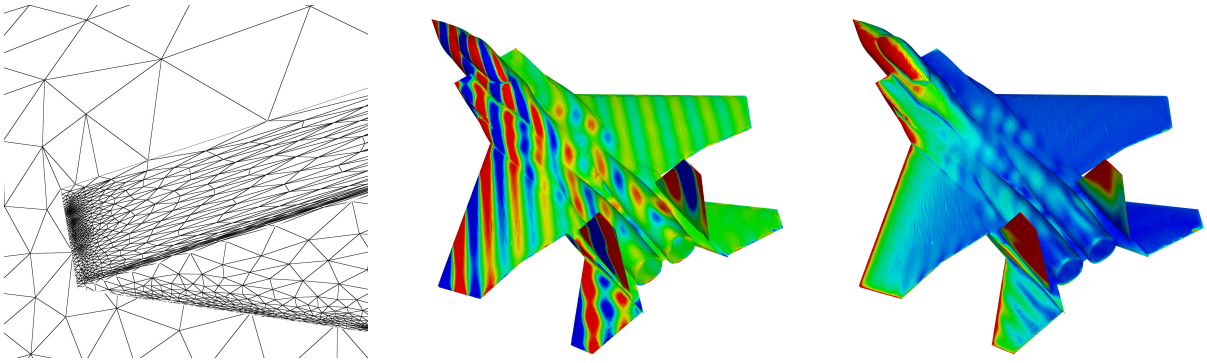

FIGURE 5 – *Diffraction by an F-15 aircraft :a portion of the adapted mesh where a wing meets the body ; the real part of the boundary solution ; and the complex amplitude of the boundary solution for* $k = 6$.

To evaluate the gain of using an anisotropic approach, an isotropic and uniform mesh have been generated with the same level of discretization as its anisotropic counterpart. The factors provided in Table 1 are the multiplication factors at each iteration of the adaptation process needed to obtain the sizes of the isotropic and uniform meshes, respectively. We observe that if an isotropic approach was used, the size of the meshes would be approximately 3 times greater. And if uniform meshes were employed, the size of the meshes to achieve the same accuracy would be between 300 and 6 million times greater ! For instance, the uniform mesh having the same accuracy than the 15th mesh is composed of more than 500 million vertices. This illustrates the optimality of the anisotropic approach to reduce CPU times.

Iteration	Minimal Size	Gain over isotropic	Gain over uniform
3	$9 \cdot 10^{-3}$	3.9	378
6	$4 \cdot 10^{-3}$	4.9	2 535
9	$1.3 \cdot 10^{-3}$	3.0	47 572
12	$5.6 \cdot 10^{-4}$	3.2	377 246
15	$1.8 \cdot 10^{-4}$	3.5	6 195 211

TABLE 1 – *F15 aircraft : Expected gain in terms of DOFs of using an anisotropic approach compared to isotropic or uniform refinement.*

If this mesh adaptation strategy is very efficient in terms of the convergence with respect to the number of degrees of freedom, it opens some new challenges for the BEM solver such that we are not yet able to consider the configuration of Figure 1. Unfortunately, such heavily non-uniform discretizations (with stretched elements next to regular elements) lead to poorer conditioning of the FM-BEM system, motivating the need for an efficient preconditioned iterative solver. Hence, the iteration count of the iterative solver becomes now the main limitation to consider realistic problems. The definition of efficient preconditioners for fast BEMs is a timely and difficult subject since the system matrix is never explicitly assembled. Standard preconditioning strategies proposed in the context of FEM cannot then be transposed to the BEM context.

A third originality of our work is to use the complementary aspects of two fast BEMs : the fast multipole method and hierarchical-matrix based BEMs ($\mathcal{H}$-BEMs) [6] to define an efficient preconditioner. These approaches are usually considered to be competitors while they have complementary advantages and drawbacks. Our overall aim is to reduce total computational cost of the adaptive FM-BEM. Since the FM-BEM solvers have been shown to have an optimal complexity for wave propagation problems, our goal is to supplement the FM-BEM with a preconditioning provided by a $\mathcal{H}$-matrix representation of the BEM system. The principle of H-matrices is to partition the initial dense linear system and reduce it to a data-sparse one by finnding sub-blocks in the matrix that can be accurately approximated by low-rank matrices. The efficiency of hierarchical matrices relies on the possibility to approximate, under certain conditions, the underlying kernel function by low-rank matrices. The approach has been

shown to be very efficient for asymptotically smooth kernels (e.g., the elastostastic kernel) and relatively efficient in a large frequency range for oscillatory kernels such as Helmholtz or elastodynamic kernels. These two approaches have advantages and drawbacks in the context of the acceleration of BEMs. On the one hand, H-matrix based BEMs (H-BEM) are very easy to implement and have the advantage to be an algebraic approach. Most of the computational time of H-BEMs is spent to evaluate the data-sparse approximation of the BEM matrix, the cost of a matrix-vector is then very cheap. On the other hand, Fast Multipole accelerated BEMs (FM-BEMs) have been shown to have an optimal complexity in terms of computational times and memory requirements for wave propagation problems. The counterpart is a more involved implementation effort. We will use a two level GMRES. The inner GMRES is used to calculate the preconditioner while the outer GMRES solves the corresponding preconditioned system.

The setup and single-iteration times for the F15 problem are presented in Figure 6. We can observe that the addition of an $\mathcal{H}$-matrix construction for the nested preconditioning results in a slightly longer precomputation time. The single iteration times are longer as well since they include an FMM matrix-vector computation as well as inner $\mathcal{H}$-matrix computations. The global time-to-solution given in Table 2, however, is significantly less for the preconditioned FM-BEM solver owing to the significant reduction in the number of overall (outer) GMRES iterations when resolving the FM-BEM system, enabling up to more than 80% reduction in global computation time.

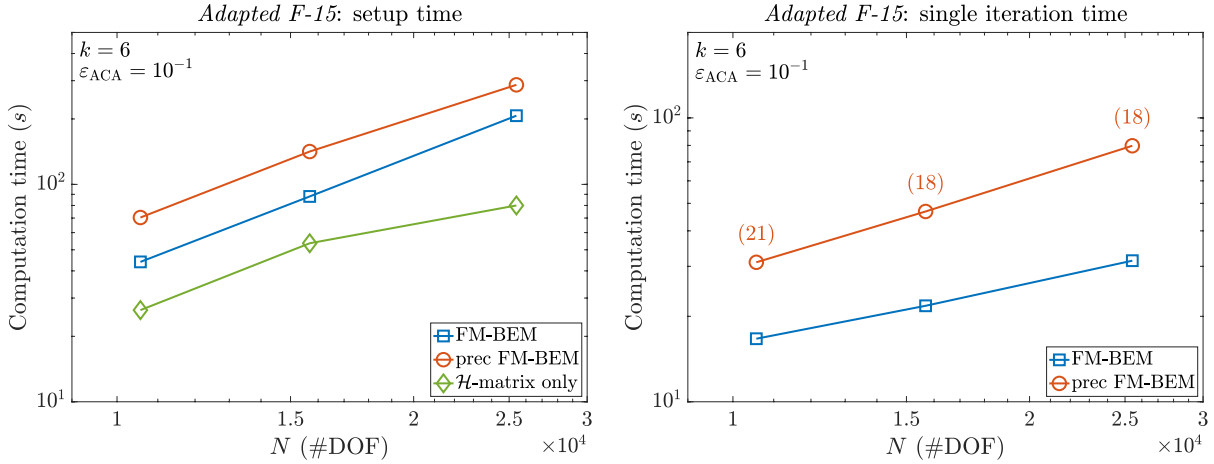

FIGURE 6 – *Diffraction by an anisotropically discretized F-15 aircraft : setup times (t_{setup},t^{prec}_{setup}) and single iteration times (t_{iter},t^{prec}_{iter}) for wavenumber $k = 6$. The maximum numerical rank along all admissible blocks in the $\mathcal{H}$-matrix representation is given in parentheses.*

N	Min length	Max length	γ_{mean}	γ_{max}	N_{iter}	t_{global}	$N^{\text{prec}}_{\text{iter}}$	$t^{\text{prec}}_{\text{global}}$	S
10562	$2.96 \cdot 10^{-3}$	$9.51 \cdot 10^{-1}$	$2.03 \cdot 10^{2}$	$3.21 \cdot 10^{2}$	210	59m06s	18	10m19s	83%
15687	$1.97 \cdot 10^{-3}$	$8.23 \cdot 10^{-1}$	$3.22 \cdot 10^{2}$	$4.18 \cdot 10^{2}$	180	66m48s	21	18m23s	73%
25428	$9.75 \cdot 10^{-4}$	$1.14 \cdot 10^{-0}$	$7.44 \cdot 10^{2}$	$1.17 \cdot 10^{3}$	180	97m41s	25	38m22s	61%

TABLE 2 – *Diffraction by an F-15 aircraft : number of solver iterations and global solution times (including setup) for wavenumber $k = 6$.*

5 Conclusion and future work

Mesh adaptation for BEMs is an important topic but the interest on this subject is new and limited to a small community. The main originality of our mesh adaptation procedure is to be metric-based and to lead to completely anisotropic meshes whereas other existing approaches lead to isotropic meshes. The method proposed is independent of the PDE (e.g. acoustics or elastodynamics), discretization technique (e.g., collocation, Galerkin) and independent of the complexity of the geometry. It completely remeshes at each refinement step, altering the shape, size, and orientation of elements according to the optimal metric based on a numerically recovered Hessian of the boundary solution. The resulting adaptation is

truly anisotropic and we have shown via numerical examples that it recovers optimal convergence rates for domains with geometric singularities.

The counterpart when using anisotropic meshes is a deterioration of the conditioning of the FM-BEM system motivating the proposition of an efficient preconditioner. It relies on an inner GMRES sequence of coarse and very fast $\mathcal{H}$-matrix approximated matrix-vector products to precondition the FM-BEM system used in the outer GMRES. We have demonstrated a reduction in the (outer) GMRES iterations and hence the subsequent invocations of the more expensive FM-based matrix-vector product, resulting in significant global time-to-solution speedups versus standard FM-BEM.

These first encouraging anisotropic BEM results pave the way for further developments. The first important future direction is to improve the treatment of curved surfaces. It has been observed numerically that the level of anisotropy must be controlled to ensure a good approximation of the scatterer surface. For complex geometries, a more thorough method needs to be employed. Another important improvement concerns the FMM. The version employed in this work is not optimal with respect to computational times for non uniform meshes. It would be of interest to employ an FMM which is tailored to the adapted meshes. Further work will also involve adapting the H-matrix construction specifically for highly anisotropic meshes. Once these points will be completely under control, we will apply the methodology to more complex problems of site effects. The idea is to optimize the repartition of the DOFs on the interface between two homogeneous layers to avoid the current approach requiring to adapt the element size to the smallest wavelength.

Références

[1] M. Ainsworth and J. T. Oden. *A posteriori error estimation in finite element analysis*, John Wiley & Sons, 2011.

[2] M. Bakry, S. Pernet, and F. Collino. *A new accurate residual-based a posteriori error indicator for the BEM in 2D-acoustics*, Computers & Mathematics with Applications, 73 : 2501–2514, 2017.

[3] A. Bespalov, T. Betcke, A. Haberl, D. Praetorius. *Adaptive BEM with optimal convergence rates for the Helmholtz equation*, Computer Methods in Applied Mechanics and Engineering, 346 : 260-287, 2019.

[4] M. Bonnet. *Boundary integral equation methods for solids and fluids*, John Wiley, 1995.

[5] S. Chaillat, M. Bonnet and J.F. Semblat. *A multi-level fast multipole BEM for 3-D elastodynamics in the frequency domain*. Comput. Methods Appl. Mech. Engrg., 197 : 4233–4249, 2008.

[6] S. Chaillat, L. Desiderio, P. Ciarlet. *Theory and implementation of $\mathcal{H}$-matrix based iterative and direct solvers for Helmholtz and elastodynamic oscillatory kernels*, Journal of Computational Physics, 351, 165-186, 2017.

[7] S. Chaillat, S.P. Groth, A. Loseille. *Metric-based anisotropic mesh adaptation for 3D acoustic boundary element methods*, Journal of Computational Physics, 372, 473-499, 2018.

[8] A. Loseille and F. Alauzet. *Continuous mesh framework part I : well-posed continuous interpolation error.* SIAM Journal on Numerical Analysis, 49 : 38–60, 2011.

[9] J.F. Semblat, A. Pecker. *Waves and vibrations in soils : earthquakes, traffic, shocks, construction works*, IUSS Press, 2009.